NUCLEAR SCIENCE AND TECHNIQUES **25**, 050302 (2014)

Biological characteristics of [^{18}F]-THK523 for tau imaging*

KONG Yan-Yan (孔艳艳),[1] SI Zhan (司展),[1] ZHANG Zheng-Wei (张政伟),[1] GUAN Yi-Hui (管一晖),[1,†] CAO Guo-Xian (曹国宪),[2] XUE Fang-Ping (薛方平),[1] HUA Feng-Chun (华逢春),[1] WU Ping (吴平),[1] ZHAO Jun (赵军),[1] ZHU Jian-Hua (朱建华),[3] LI Cong (李聪),[3] CHEN Jian (陈键),[3] and QIAN Jun (钱隽)[3]

[1]*PET Center, Huashan Hospital, Fudan University, Shanghai 200235, China*
[2]*Key Laboratory of Nuclear Medicine, Ministry of Health, Jiangsu Key Laboratory of Molecular Nuclear Medicine, Jiangsu Institute of Nuclear Medicine, Wuxi 214063, China*
[3]*Key Laboratory of Smart Drug Delivery, Ministry of Education & PLA, School of Pharmacy, Fudan University, Shanghai 200032, China*

(Received January 7, 2014; accepted in revised form February 21, 2014; published online October 4, 2014)

Reliable and non-invasive diagnostic tools are highly valuable for successful therapeutic strategies for the treatment of Alzheimer's disease (AD). The existence of neurofibrillary tangles (NFTs) consisting of tau protein are one kind of the pathological features of AD, and its level of severity is correlated with the stage of AD. However, no clinically approved positron emission tomography (PET) probe is currently available for selective imaging of neurofibrillary tangles on patients. In this paper, we report our studies on biological characteristics of [^{18}F]-THK523 as a novel tau imaging probe. With low molecular weight, [^{18}F]-THK523 is stable, electrically neutral, lipophilic and non-mass concentration-dependent. Preliminary biological studies have shown the excellent properties of [^{18}F]-THK523 as brain imaging tracer for further research.

Keywords: [^{18}F]-THK523, Neurofibrillary tangles (NFTs), Alzheimer's disease (AD), Tau-specific probe, Biological characteristics

DOI: 10.13538/j.1001-8042/nst.25.050302

I. INTRODUCTION

National Institute on Aging-Alzheimer's Association (USA) has suggested that Alzheimer's disease (AD) would be optimally treated before significant cognitive impairment, defined as a 'presymptomatic' or 'preclinical' stage [1]. Diagnosis and treatment strategies for AD are based on sensitive and specific detection of the incipient neuropathological characteristics, combined with emerging treatments that counteract molecular processes in AD pathogenesis. The hyperphosphorylation of tau protein and formation of intraneuronal neurofibrillary tangles (NFTs) represent a characteristic neuropathological feature in AD brain.

Tau, localizing in the axons of neurons, is a microtubule-associated protein (MAP) and maintains microtubules (MTs) stability, neurite outgrowth and chromosome stability [2–5]. NFTs are constituent of aggregated paired helical filaments (PHF) comprising of aberrantly phosphorylated tau. NFTs are formed in entorhinal cortex at the early stage of AD, and spread to the dentate gyrus, hippocampus, and cingulate cortex as the memory loss develops [6]. NFTs, especially soluble hyperphosphorylated tau aggregations, interact with Aβ-mediated toxicity, oxidative stress, inflammation and abnormal mitochondrial function [7, 8]. Also, anti-tau treatment can reduce Aβ formation and the excitotoxicity levels [9, 10].

The utility of positron emission tomography (PET), with a radio-ligand for translocator protein as a biomarker for tau-triggered toxicity tau imaging and diagnostic assessment of tauopathies, with and without Aβ pathologies, shall be of technical importance for both clinical and basic research aimed at prodromal pathologies of AD.

There is no effective treatment target tau pathology used clinically. Nakamura *et al*. [11] reported in 2012 that unlike trans p-tau, cis isomerization p-tau by proline-directed kinases appeared early in the brains of humans with mild cognitive impairment, accumulated exclusively in degenerated neurons, and localized to dystrophic neuritis during AD progression. Cs isomer cannot promote MTs assembly. It is more resistant to dephosphorylation and degradation, and more prone to aggregation. Conventional peptidyl-prolyl cis-trans isomerases (PPIases) Pin1 can convert *cis* to *trans* p-tau to prevent Alzheimer's tau pathology. Tau-specific PET probe can effectively evaluate such new approach with accurate, reliable, and reproducible noninvasive monitoring of tau protein aggregates in the living brain.

There has been an increasing focus on developing PET imaging radiotracers for preclinical diagnosis of AD, especially [^{18}F]-THK523, which may be a potential tau targeted probe. *In vitro* binding studies demonstrated that [^{18}F]-THK523 had higher affinity to a greater number of binding sites on recombinant tau (k18Δ280k) than β-amyloid$_{1-42}$ fibrils. [^{18}F]-THK523 bound to tau pathology on autoradiographic and histofluorescence analysis of AD hippocampal serial sections. It had higher retention in tau transgenic mice brain than wild-type littermates mice, and that it bound to recombinant tau with much higher affinity than it did to β-amyloid plaques [12]. And it showed higher affinity to

* Supported by National Natural Science Foundation of China (Nos. 81271516 and 81371625), Program of Shanghai Science and Technology Commission (Nos. 13JC1401503 and 14DZ1930402), Shanghai Municipal Health and Family Planning Commission (No. 2013313) and Exchange Programme Foundation of Doctoral Student under the Office for Graduate Medical Education, Fudan University
† Corresponding author, guanyihui@hotmail.com

tau fibrils than Aβ fibrils by comparing the binding properties of [^{18}F]-THK523 and other amyloid imaging agents, including PiB, BF-227 and FDDNP, to synthetic protein fibrils and human brain tissue [13]. Zeng *et al*. [14] demonstrated that [^{3}H]-THK523 binds to NFTs and Aβ plaques in human AD brain sections. However, in transgenic mouse brain sections, [^{3}H]-THK523 binds only to Aβ but fails to bind to NFTs. Okamura *et al*. [15] reported that novel ^{18}F-labeled arylquinoline derivatives, ^{18}F-THK-5105 and ^{18}F-THK-5117, had higher binding affinity for tau protein aggregates and tau-rich AD brain homogenates, and higher brain uptake and faster clearance in normal mice than [^{18}F]-THK523. In this paper, we report our complementary biological characteristics studies to investigate whether [^{18}F]-THK523 can meet ligand criteria for tau imaging tracer.

II. MATERIALS AND METHODS

A. Labeling procedure

The 2-((2-(4-(*tert*-butoxycarbonyl)amino)phenyl)quinolin-6-yl)oxy)ethyl 4-methylbenzenesulfonate (THK-7), as protected precursor, was synthesized at our lab [16]. [^{18}F]-THK523 was radio-synthetized with high yield from THK-7 by a fully automated module (PET Science & Technology Co. Ltd., Beijing, China) [16]. Aqueous $^{18}F^{-}$ trapped on a quadrupole mass analyzer (QMA) cartridge was washed by 1.5 mL of K_2CO_3 (2.73 mg/mL)/Kryptofix^{TM}2.2.2 (11.82 mg/mL), and the solvents were evaporated. After 2 mg of THK dissolved in 1 mL of acetonitrile (2 mg/mL) was added, the nucleophilic substitution reaction was carried out at 120 °C. To hydrolyze the Boc protecting group, 1 N HCl (250 μL) solution was added. The mixture was allowed to react at 105 °C for 5 minutes. The excess HCl was neutralized by 2 N NaOH (125 μL). Saturated 1 N $NaHCO_3$ (125 μL) was added to adjust the pH value to 7.4. The product was loaded on a Sep-Pak tC18 SPE cartridge, and washed with water to remove free $^{18}F^{-}$, polar byproducts, Kryptofix®^{TM}2.2.2, etc. The cartridge was then washed with 2 mL of ethanol. Crude product was collected after passing through a sterile filter, followed by further purification using semipreparative high-performance liquid chromatography (Waters XBridge^{TM} prep Shield RP18 10 μm, 250 mm × 10 mm, part No. 186003990, serial No. 101/123041GG01, 70% EtOH : 30% H_2O; Waters Corporation, Milford, Massachusetts, USA) equipped with Bioscan radioactivity detector at a flow rate of 4 mL/min and stabilized with ascorbic acid (2 mg, 0.011 mmol) before sterile filtration. Quality control of [^{18}F]-THK523 was achieved by thin layer chromatography (TLC) and radio high-performance liquid chromatography (RHPLC).

Radiochemical yield of [^{18}F]-THK523 was evaluated by TLC using silica gel G60 with fluorescence (F254) plates (cut into 10 cm × 0.4 cm strips) as stationary phase while ethyl acetate : *n*-hexane : triethylamine = 4:1:0.005 ($V/V/V$) as mobile phase. The reaction product was spotted with a capillary and developed by mobile phase. After development, the strips were dried at room temperature, cut into 1 cm × 0.4 cm pieces and counted by Wizard 1470 automatic gamma counter (Perkin Elmer Company, USA) equipped with a multi-channel analyzer. Retention factor (Rf) and labeling yield were determined from TLC chromatogram data. Two TLCs ran for each tested reaction condition and the data were averaged as the labeled rate.

The radiochemical purity (RCP) of [^{18}F]-THK523 was determined by analytical RHPLC. The sample was passed through a Millipore filter carefully and then injected into the HPLC column (Purospher®STAR LPRP-18e endcapped (5 μm), 250×4.6 mm, sorbent Lot No. TA1752311, column No. 210072) at room temperature. The absorbance was measured at 350 nm and the flow rate was adjusted to 0.6 mL/min. An injection volume of 20 μL tracer was used with a mobile phase at volume (acetonitrile)/volume (containing triethylamine 0.05% water) ratio of 80%/20%. Retention time (Rt) was measured and checked with the standard product.

B. Electrophoresis

The charge of [^{18}F]-THK523 was determined by paper electrophoresis using kalium phosphate buffer solution: alcohol: distilled water, 1:1:1 ($V/V/V$) with pH 7.4 as electrolyte and Xinhua No. 1 papers strips as a support. The sample was run at a constant voltage of 110 V for 2.5 h of standing time. The strip was scanned by gamma-counter. For comparison, a sample of $^{18}F^{-}$ was run under the identical condition.

C. Determination of lipid–water partition coefficient of [^{18}F]-THK523

Lipid–water partition coefficient of [^{18}F]-THK523 was measured in two steps. Step 1: 1 mL of phosphate-buffered saline (PBS) (pH = 7.4) saturated by n-octyl alcohol and 1 mL of n-octyl alcohol saturated by PBS (pH = 7.4) were added to centrifuge tube containing 100 μL of sample. Step 2: The tube was capped and vortexed for 10 min at room temperature, and then stood for 5 min. After reaching equilibrium, the tube was centrifuged at 2000 r/min (r = 6.0 cm) for 10 min. 100 μL of the organic phase and water phase were pipetted out respectively and each phase was counted by the gamma counter. The organic phase of 500 μL was pipetted out into another centrifuge tube and then followed by the addition of 500 μL of n-octyl alcohol saturated by PBS (pH = 7.4) and 1 mL of PBS (pH = 7.4) saturated by *n*-octyl alcohol. Step 2 was repeated for six times. The partition coefficient was calculated as (*cpm in organic phase*)/(*cpm in water phase*).

D. Measurement of plasma protein binding rate

Heparin anticoagulant fresh blood plasma of 10 volunteers was provided by Nuclear Medicine Department, Huashan Hospital affiliated to Fudan University. Trichloroacetic acid with volume fraction of 10% and 25% was prepared, respectively. The experiment was divided into the high, middle,

mid-low and low dose groups, each having four parallel samples. Each tube contained 0.2 mL blood plasma and 0.1 mL of [^{18}F]-THK523 in activity of 22.20, 2.22, 0.22 or 0.02 MBq for the high, middle, mid-low and low dose groups, respectively. Being incubated for 2 hours at 37 °C, each tube was added with 1 mL of 25% trichloroacetic acid. They were vortex blended, and centrifuged at 2000 r/min (r = 6.0 cm) for 10 min. Then, the supernatant was collected. Afterwards, 1 mL of 10% trichloroacetic acid was added to the precipitate. This step was repeated twice. According to the radioactivity counts of precipitation and supernatant, plasma protein binding rate was calculated as following: *plasma protein binding rate* = [(*precipitation radioactive counts*) / (*precipitation* + *supernatant radioactive counts*)] × 100%.

E. Stability studies

Stability assessment of the complex was carried out by measuring its radio chemical purity at 25 °C. The radiochemical purity of [^{18}F]-THK523 was determined by TLC and the radioactivity of [^{18}F]-THK523 was counted by gamma counter at 0.5, 1, 1.5, 2, 3, 4, 5, 6 and 7 h after preparation.

F. Blood kinetic studies

Blood clearance studies were performed in C57 mice (n = 5, (21 ± 1) g). For each animal, 5.18 MBq/140 μCi of the [^{18}F]-THK523 (0.1 mL) was administered intravenously through the tail vein. Blood samples (10 μL) were collected from the tail vein and radioactivity was measured by the gamma counter at different time intervals (2, 5, 10, 15, 20, 30, 45 and 60 min) after intravenous injection. The data was expressed as percentage of the administered dose at each time point. The weight of each blood sample was determined by weighing the microcentrifuge tube before and after blood collection. The concentrations of radioactivity in the blood were calculated as %ID/g. The blood clearance patterns of [^{18}F]-THK523 were simulated using Pharmacokinetics Local Model (PLM) software developed by Cao *et al*. [17].

G. Micro PET Imaging

Normal C57 mice ((20 ± 2) g) were acquired with a Siemens Inveon PET/CT system (Siemens Medical Solutions, Knoxville, USA). After induction of anesthesia and placement of the catheter systems, the animals were placed with their bodies in the center of the field of view and were fixed in the scanner in prone feet first position (FFP). At the beginning of the PET scanning procedure, a CT scan (Inveon) was performed for all animals. [^{18}F]-THK523 was given via the catheter system intravenously in a slow bolus. The total applied volume was (0.18 ± 0.02) mL. The amount of injected activity was (0.15 ± 0.03) mCi. Radioactivity in the syringe and catheter was measured immediately before and after injection. Dynamic data acquisition was performed by Inveon Acquisition Workplace (IAW, Siemens) for 60 min starting immediately after injection (p.i.) of the tracer. A PET image was reconstructed from 600 million coincidental 511 keV photon counts. A reconstruction of sinograms yielded a 3D mapping of positron signal using Fourier rebinning and a 2D filtered back-projection algorithm with a ramp filter. And the voxel size was set as 0.80 mm × 0.86 mm × 0.86 mm. CT images were reconstructed using a modified Feldkamp cone beam reconstruction algorithm (COBRA) from 360 projections with isotropic pixel size of 110 μm. The emission data were normalized and corrected for decay and dead time. The resulting sinograms were reconstructed with FBP (filtered back-projection) into 8 frames (1@120; 1@180; 3@300; 1@600; 2@900) of equal length used for motion correction, ratio measurements and image production for time-activity curve (TAC) generation.

For each micro PET scan, three-dimensional regions-of-interest (ROIs) were drawn over the major organs by using vendor software (Inveon Research Workshop; IRW) on decay-corrected whole-body images. All PET and CT image datasets were scaled to calibrated kBq/cc and saved in float format. Orientation of planes was confirmed to radiological human brain standard such that the Z-axis was perpendicular to horizontal sections.

To retrieve reliable small-animal PET results, accurate and standardized co-registration of PET to CT is essential. A two-step matching process of PET data was used. The initial automatic rigid matching was performed first, and manual adjustment was applied if necessary. High-resolution CT scan was used as the basis for VOI definition. To quantify the dynamic data, TACs with high initial time resolution were used.

H. Biodistribution studies in mice

Ex vivo biodistribution studies were carried out to confirm that the quantitative tracer uptake values based on non-invasive micro PET imaging truly represented the actual tracer distribution in normal mice. Fifty C57 mice ((20 ± 2) g) from Shanghai Slac Laboratory Animal CO. Ltd. were used in animal experiments (25 female, 25 male). They were divided into ten groups randomly according to sacrifice time points. [^{18}F]-THK523 (0.1 mL) in activity of 5.18 MBq/140 μCi was injected into the tail vein of each mouse and the animals were sacrificed at 2, 5, 10, 15, 30, 45, 60, 120, 180 and 240 min after injection. Samples of the major organs/tissues of interest, including liver, spleen, pancreas, stomach, intestine, femur, muscle, gonad, lung, kidney, heart, brain and blood, were collected and wet-weighed. Specific radioactivity of the tissue samples was measured using a gamma-counter. The percent dose per organ was calculated by a comparison of the tissue counts to the counts of a suitably diluted aliquot of the injected material. The concentrations of radioactivity in the blood were also calculated as %ID/g.

The experiments were carried out in compliance with national laws for the conduct of animal experimentation and were approved by the local committee for animal research.

III. RESULTS

A. Electrophoresis

Charge of the complex was confirmed by paper electrophoresis. Table 1 shows that 95.8% of [^{18}F]-THK523 stay still under the condition of current, indicating that it was electrically neutral; while the ^{18}F- species moved to anode, indicating that the compound exhibited anionic behavior.

TABLE 1. Electrophoresis of [^{18}F]-THK523

Samples	Percentage radioactivity		
	Anode	Spotting	Cathode
^{18}F-THK523	2.3	95.8	1.9
$^{18}F^-$	94.7	3.2	2.1

B. Determination of lipid–water partition coefficient of [^{18}F]-THK523

The lipophilicity of [^{18}F]-THK523 is determined by lipid–water partition coefficient ($\lg P$), and the results are listed in Table 2 ($\lg P = 0.99 \pm 0.06$, $n = 7$), indicating [^{18}F]-THK523 is lipophilic, which is consistent with Ref. [12, 13].

TABLE 2. Lipid-water partition coefficient of [^{18}F]-THK523

γ-counts (cpm/0.5 mL) ($n = 7$)		n-octanol/PBS	$\lg P$
n-octanol	PBS		
643684	75619	8.5122	0.9300
287112	25748	11.1508	1.0473
160896	20857	7.7142	0.8873
84093	8091	10.3934	1.0168
40947	3978	10.2934	1.0126
19726	1764	11.1825	1.0485
9996	1041	9.6023	0.9824

C. Measurement of plasma protein binding rate

Plasma protein binding rate was (8.68±0.45)%, (7.86±0.32)%, (8.13±0.35)% and (8.11±0.53)% for the high, middle, mid-low and low concentration groups, respectively. They do not differ significantly, indicating that the protein binding rate of [^{18}F]-THK523 is not of the mass concentration-dependent nature.

D. Stability studies

Stability of the radiolabeled compound over time was investigated. According to our test results, radiochemical purity of [^{18}F]-THK523 was stable, remaining at the level of about 90% for up to 5 h. It was decreased to 87.6% and 86% at 6 h and 7 h respectively (Fig. 1). Considering the radioactive decomposition and decay of ^{18}F, it is better to applied [^{18}F]-THK523 within 5 h after preparation.

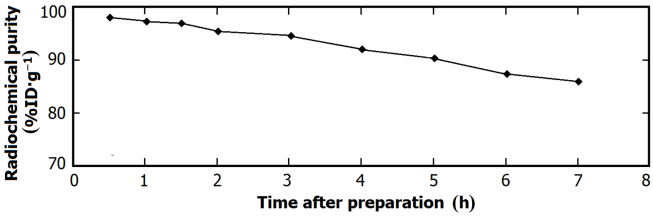

Fig. 1. Stability of [^{18}F]-THK523 at room temperature.

E. Blood kinetic studies

The following dual-exponential equation was adopted to model the pharmacokinetic of [^{18}F]-THK523 in mice in mice: $Y = 2.23e^{-0.014t} + 1.89^{-0.0007t}$, where Y is %ID g^{-1} in blood; t is time in minute. The distribution and elimination were coincident with the results given by compartment modeling. The pharmacokinetics parameters of [^{18}F]-THK523 are listed in Table 3.

TABLE 3. Pharmacokinetic parameters of [^{18}F]-THK523 in mice (131.35 MBq/mL, $n = 5$)

Parameters	[^{18}F]-THK523
Distribution-phase half-time, $t_{1/2\alpha}$ (min)	47.9247
Elimination-phase half-time, $t_{1/2\beta}$ (min)	965.1007
Transfer rate constant from peripheral compartment to the central compartment, K_{21} (min^{-1})	0.0070
Eliminate constant, K_e (min^{-1})	0.0015
Transfer rate constant from central compartment to the peripheral compartment, K_{12} (min^{-1})	0.0067
Apparent volume of distribution, V_d (mL)	50.0037
Area under CTC[a], AUC (ID%/g/min)	2785.0782
Plasma clearance, CL (ID%/g/min)	0.0359

[a] CTC, concentration-time curve

F. Micro PET imaging and Biodistribution studies in mice

The biodistribution of [^{18}F]-THK523 was determined *ex vivo* in healthy mice at 2, 5, 10, 15, 30, 45, 60, 120, 180 and 240 min after intravenous injection. The uptakes in liver ((7.96 ± 0.97) %ID/g), kidney ((4.32 ± 0.33) %ID/g) and heart ((4.18 ± 0.28) %ID/g) were the highest initially at 2 min, followed by fast clearance (Fig. 2(a)). Preclinical study showed that the highest [^{18}F]-THK523 uptake occurred in gall bladder, followed by liver, kidney, heart and intestine, whereas femur and gonads showed the lowest uptake (Fig. 2(b)). Within less than 15 min, [^{18}F]-THK523 essentially cleared from blood and plasma. [^{18}F]-THK523

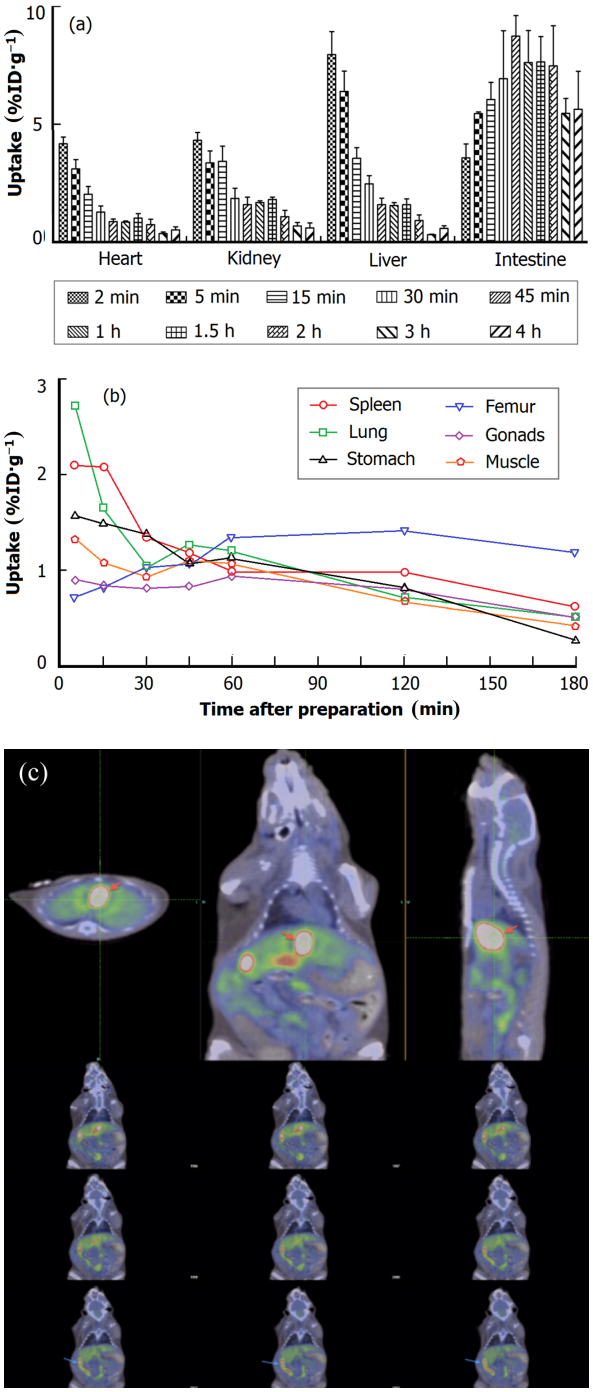

Fig. 2. (Color online) Biodistribution of [^{18}F]-THK523 in main metabolic organs (a) and other organs (b) in normal mice, and small-animal PET images of a mouse at 60 min after [^{18}F]-THK523 injection. The orange arrows indicate gall bladder, and the blue arrows indicate intestine. The data are expressed as means $\pm$ *SD* ($n = 5$).

was mainly metabolized by liver and excreted through biliary, thus leading to substantial rise in the uptake in intestine at 15 min and then slow decline started approximately at 120 min. Micro PET imaging demonstrated such changes vividly *in vivo*, agreeing with the biodistribution analysis *ex vivo* (Figs. 2(a) and 2(c)). The bone uptake rose and then decreased slowly because of radioactive decomposition, which could be improved with the presence of ascorbic acid (2 mg, 0.011 mmol).

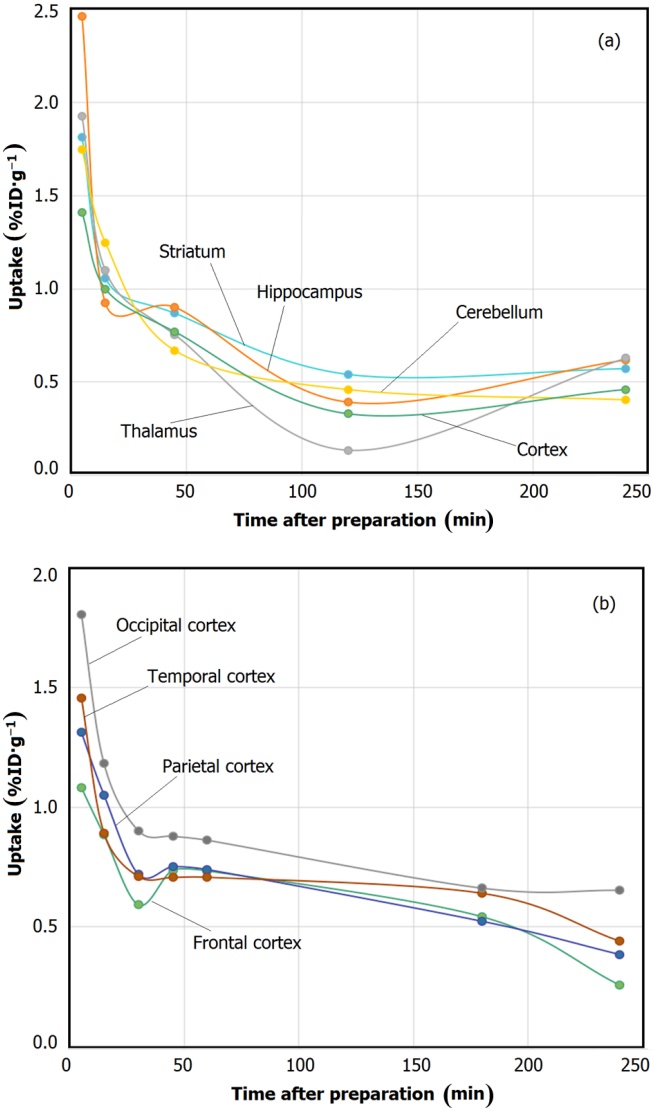

Fig. 3. (Color online) Biodistribution of [^{18}F]-THK523 in main regions (a) and cortex of in normal mice brain (expressed as means, $n = 5$).

The brain uptake was (2.62 ± 0.39) %ID/g at 2 min after injection. Mouse brains were dissected into following regions: cortex (front cortex, parietal cortex, temporal cortex, occipital cortex), striatum, hippocampus, thalamus, cerebellum, pons and medulla oblongata. The uptakes in occipital cortex ((4.91 ± 0.94) %ID/g), temporal cortex ((3.33 ± 0.72) %ID/g) and hippocampus ((3.07 ± 0.35) %ID/g) were the highest initially at 2 min, followed by fast clearance (Figs. 3(a) and 3(b)). The tracer uptake for the occipital cortex and temporal cortex were higher than other cortex (Fig. 3(b)). The brain uptake trend of [^{18}F]-THK523 was similar between *ex vivo* and *in vivo* from injec-

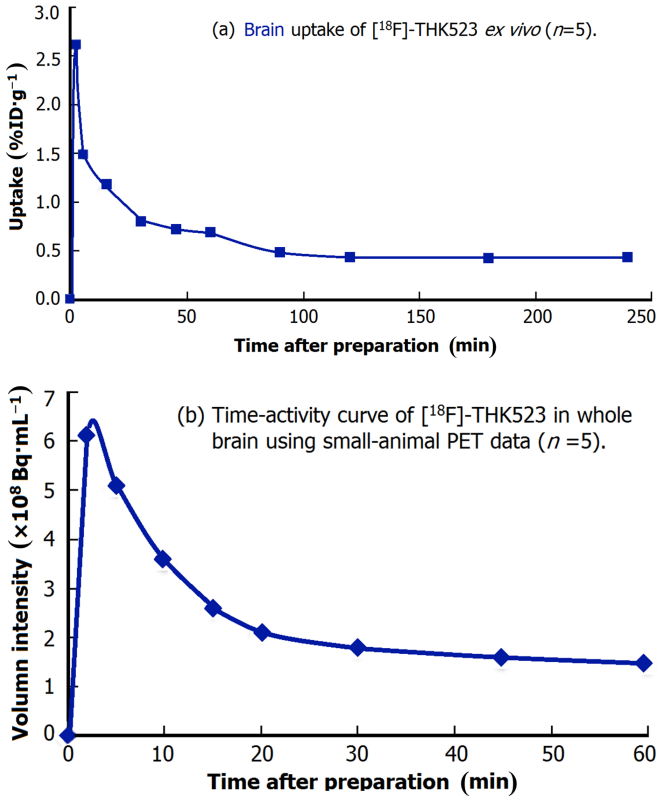

Fig. 4. (Color online) The brain uptake trend of [^{18}F]-THK523 over time in normal mice *ex vivo* (a) and *in vivo* (b).

tion to 60 min. The highest brain uptake was at 2 min after injection, followed by quick clearance during 90 min post-injection. The clearance was relatively slow from 90 min to 240 min after injection (Fig. 4).

IV. DISCUSSION

NFTs are one kind of the pathological hallmarks found in AD brains and are closely associated with the severity of dementia, indicating the contribution of NFTs to neuronal dysfunction. NFTs are therapeutic target of AD for disease modifying therapy. A PET tracer for imaging NFTs in the brain shall be valuable in developing new therapies for AD.

Considering the factors related to brain uptake, a radioactive tracer can hardly cross the blood-brain barrier (BBB) if it is not electrically neutral or non-lipophilic. For brain tracer, low plasma protein binding rate is also critical to brain uptake. If plasma protein binding rate is too high, the tracer would be unable to get access to target region. The analytical data and favorable lg P suggest that [^{18}F]-THK523 should cross the BBB and enter the central nervous system (CNS). Also, with the presence of ascorbic acid, [^{18}F]-THK523 is stable at room temperature up to 5 h. All these biological characteristics demonstrate that [^{18}F]-THK523 satisfies the basic requirements of brain tracer. Our blood kinetic studies show that [^{18}F]-THK523 distributes quickly from blood to other organs ($t_{1/2\alpha}$ = 47.9 min), with relatively favorable retention time in target organs ($t_{1/2\beta}$ = 965.1 min).

Metabolism and biodistribution patterns should be evaluated for any radiopharmaceutical candidate being considered for clinical translation. Our *ex vivo* studies reveal a high brain uptake at 2 min after injection, especially in the hippocampus, followed by rapid clearance in healthy mice. *In vitro* and *in vivo* studies have confirmed that [^{18}F]-THK523 is of high affinity and selectivity for tau pathology [12, 13], and our biological characteristics results shall help fulfilling its brain ligand criteria for further imaging trials.

V. CONCLUSION

[^{18}F]-THK523 was radiosynthesized on automated module and its biological characteristics were evaluated. *In vitro* studies demonstrated that [^{18}F]-THK523 was electrically neutral, lipophilic (lg P = 0.99 ± 0.06, n = 7) and quite stable with its radiochemical purity of more than 90% maintained for up to 7 h at room temperature. Due to its low molecular weight, [^{18}F]-THK523 can easily cross blood brain barrier (BBB). With relatively low plasma protein binding rate, [^{18}F]-THK523 is not of mass concentration-dependent nature. From calculations of pharmacokinetics parameters of the blood, and the blood kinetic study, the dual-exponential equation was $Y = 2.23e^{-0.014t} + 1.89^{-0.0007t}$ with $t_{1/2\alpha}$ = 47.9 min^{-1}, $t_{1/2\beta}$ = 965.1 min^{-1}, K_{12} = 0.0067 min^{-1}, K_{21} = 0.0070 min^{-1}, K_e = 0.0015 min^{-1}, plasma clearance = 0.036 %ID/g/min, area under concentration-time curve = 2785.1 ID%/g/min. [^{18}F]-THK523 is of high brain uptake, and our study on its biodistribution in healthy C57 mice shows that [^{18}F]-THK523 is mainly metabolized by liver and excreted through biliary. [^{18}F]-THK523 may well be a promising candidate for molecular imaging of tau pathology.

ACKNOWLEDGEMENTS

We are grateful to GAO Xi-Hui, HUANG Cui-Yun, ZHENG Shu-Yan and WANG Feng for helpful brain anatomy and counseling in all aspects of animal handling and experimenting.

[1] Mori T, Maeda J, Shimada H, *et al*. Psychogeriatrics, 2012, **12**: 106–114.
[2] Wang J Z and Liu F. Prog Neurobiol, 2008, **85**: 148–175.
[3] Rossi G, Dalprà L, Crosti F, *et al*. Cell Cycle, 2008, **7**: 1788–1894.

[4] Witman G B, Cleveland D W, Weingarten M D, *et al*. Proc Natl Acad Sci USA, 1976, **73**: 4070–4074.
[5] Guo J L, Covell D J, Daniels J P, *et al*. Cell, 2013, **154**: 103–117.
[6] de Calignon A, Polydoro M, Suarez-Calvet M, *et al*. Neuron, 2012, **73**: 685–697.
[7] Revett T J, Baker G B, Jhamandas J, *et al*. J Psychiatr Neurosci, 2013, **38**: 6–23.
[8] Ittner L M, Ke Y D, Delerue F, *et al*. Cell, 2010, **142**: 387–397.
[9] Roberson E D, Scearce-Levie K, Palop J J , *et al*. Science, 2007, **316**: 750–754.
[10] Nussbaum J M, Schilling S, Cynis H, *et al*. Nature, 2012, **485**: 651–655.
[11] Nakamura K, Greenwood A, Binder L, *et al*. Cell, 2012, **149**: 232–244.
[12] Fodero-Tavoletti M T, Okamura N, Furumoto S, *et al*. Brain, 2011, **134**: 1089 –1100.
[13] Harada R, Okamura N, Furumoto S, *et al*. Eur J Nucl Med Mol, 2013, **40**: 125–132.
[14] Zeng Z, Chen T B, Miller P, *et al*. Alzheimers Dement, 2012, **8**: P66.
[15] Okamura N, Furumoto S, Harada R, *et al*. J Nucl Med, 2013, **54**: 1420–1427.
[16] Kong Y Y, Cao G X, Zhang Z W, *et al*. Nucl Sci Tech, 2014, **25**: 040302.
[17] Cao G, Zhou X, Kong Y, *et al*. Nucl Tech, 2013, **36**: 60–65. (in Chinese)